SUPPORTING INFORMATION

Energy-Saving Hydrogen Production by Water Splitting Coupling Urea Decomposition and Urea Oxidation Reaction

Zehao Xiao,[#a] Yinyin Qian,[#c,d,e] Tianhui Tan,[a] Hongxiu Lu,[a] Canhui Liu,[a] Bowen Wang,[a] Qiang Zhang,[d] Muhammad Tariq Sarwar,[c,d] Ruijie Gao,[*c,d,e] Aidong Tang,[*a,c,d,e] Huaming Yang[*b,c,d,e]

[a] College of Chemistry and Chemical Engineering, Central South University, Changsha 410083, China

[b] Hunan Key Lab of Mineral Materials and Application, School of Minerals Processing and Bioengineering, Central South University, Changsha 410083, China

[c] Engineering Research Center of Nano-Geomaterials of Ministry of Education, China University of Geosciences, Wuhan 430074, China

[d] Faculty of Materials Science and Chemistry, China University of Geosciences, Wuhan 430074, China

[e] Key Laboratory of Functional Geomaterials in China Nonmetallic Minerals Industry, China University of Geosciences, Wuhan 430074, China

Chemicals

All chemicals used in this study were of analytical grade without further purification. KOH and urea were purchased from Sinopharm Chemical Reagent Co. Ltd.; $Ni(NO_3)_2 \cdot 6H_2O$ was purchased from Macklin Ltd.; $(NH_4)_6Mo_7O_{24} \cdot 2H_2O$ was purchased from Macklin Ltd.; $Na_2S \cdot 9H_2O$ was purchased from Sinopharm Chemical Co. Ltd; NH_4F was purchased from Macklin Co. Ltd; Nickel foams (NF, areal density 350 g·cm^{-2}, 1.5 mm thick) were purchased from Lvchuang Technology Co. Ltd.; hydrochloric acid (36.5%) was purchased from Chronchem Ltd. De-ionized (DI, 18.2 Ω·cm^{-1}) water was standard solution.

Synthesis of 20 wt% Pt/C/NF

10 mg commercial 20 wt% Pt/C powders, 500 μL ethanol, 460 μL water and 40 μL Nafion were uniformly dispersed in the mixture solution with ultrasonication for 1 h. Next, above dispersive solution was slowly dropped into the cleaning NF and dried in air to prepare the 20 wt% Pt/C/NF catalyst.

Synthesis of MoNi$_4$/MoO$_{3-x}$ catalyst

A piece of cleaning NF was firstly immersed into the solution of 1.2 mmol $Ni(NO_3)_2 \cdot 6H_2O$, 0.3 mmol $(NH_4)_6Mo_7O_{24} \cdot 4H_2O$ and 30 ml of DI water with stirring for 20 mins in a Teflon autoclave. The above mixed solution was then kept at 150 °C for 6 h. After the temperature reduced to room temperature, yellow $NiMoO_4$ precursor was washed for several times and dried in air at 60 °C overnight. Subsequently, the as-prepared $NiMoO_4$ precursor was placed in a tube furnace under H_2/Ar (v/v, 10/90, 100 sccm) atmosphere. The furnace was kept at 400 °C for 2 h under the heating rate of 5 °C·min^{-1}. After the temperature reduced to room temperature, black MoNi$_4$/MoO$_{3-x}$ catalyst was obtained.

DFT calculations

All theoretical calculations were carried out by the Dmol^3 software based on density functional theory (DFT). Specifically, exchange-correlation interactions were calculated by the generalized gradient approximation (GGA) with the Perdew-Burke-Ernzerhof (PBE).[1] Double numerical basis sets including polarization functions on all atoms were employed and the real-space global orbital cut-off radius was set as 4.5 Å. To avoid artificial interactions between the film and the periodic images, a vacuum space with a thickness of 25 Å was used. The weak interaction of van der Waals taken into account by using the DFT-D2 method. A 6 × 6 × 1 Monkhorst-Pack k-point sampling and the further increase in k-points had no significantly effect on the results.[2] The structure optimization reached convergence until maximum force convergence threshold of 2×10^{-3} hartree·Å^{-1}, energy differences were converged within 1.0×10^{-5} hartree·Å^{-1}, and maximum atomic displacement within 5×10^{-3} Å.
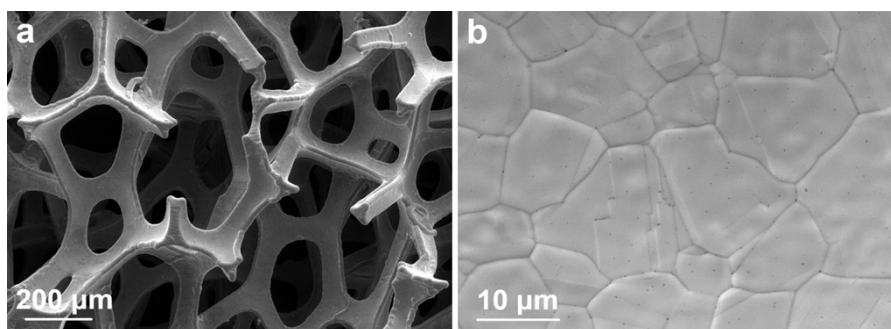

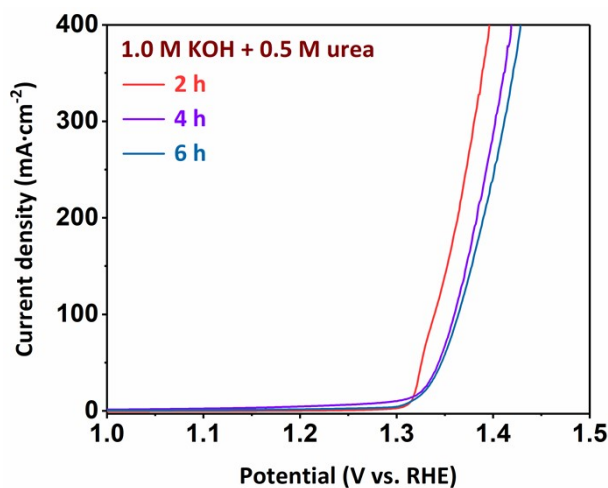**Figure S1.** SEM images of the bare NF.

Figure S2. LSV curves of the Ni_3S_2 catalyst synthesized under different sulfurization times in 1.0 M KOH with 0.5 M urea.
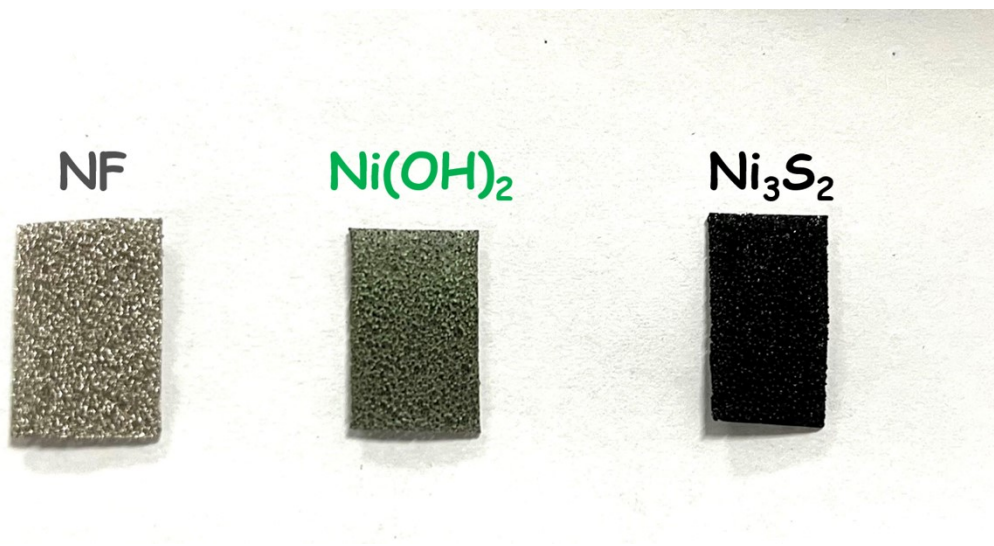

Figure S3. Digital images of NF, $Ni(OH)_2$ and Ni_3S_2.

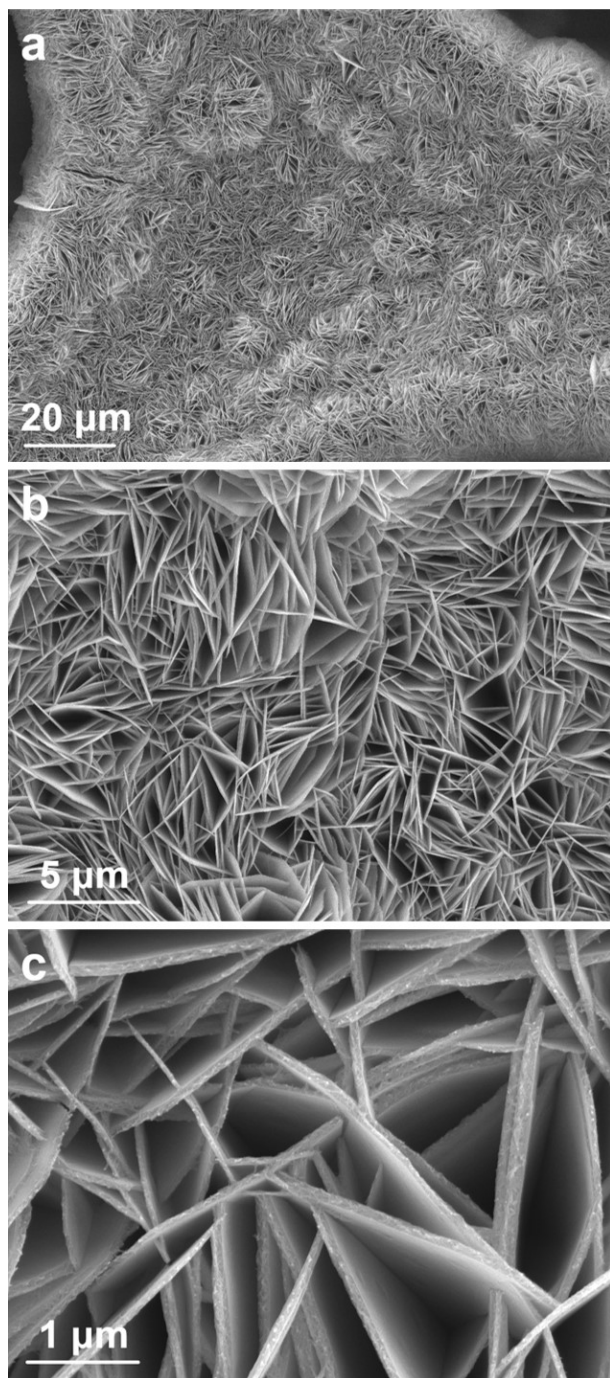**Figure S4.** SEM images of the Ni(OH)$_2$ precursor.
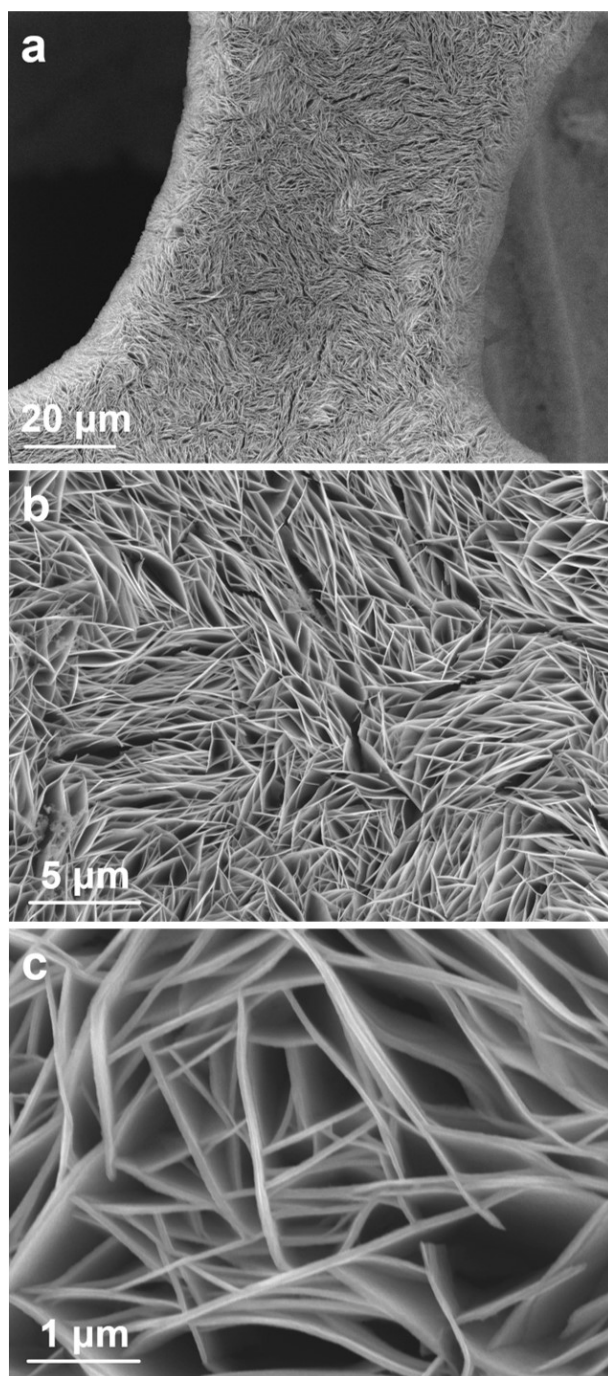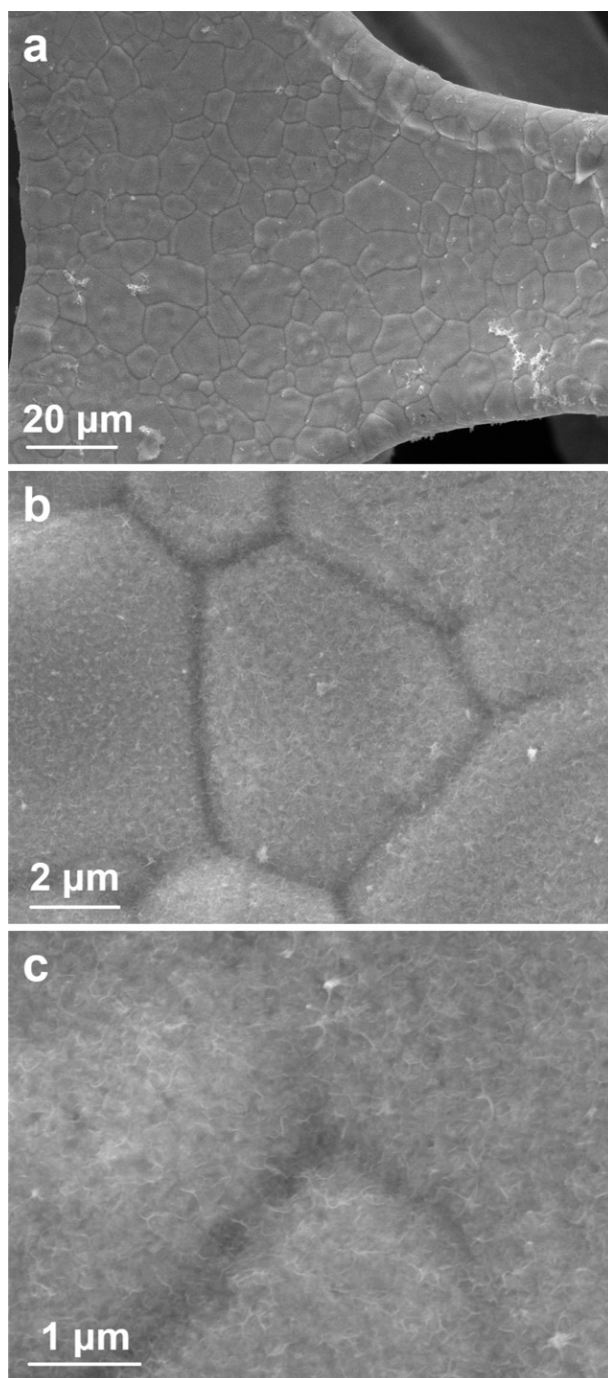
Figure S5. SEM images of the Ni_3S_2 catalyst.

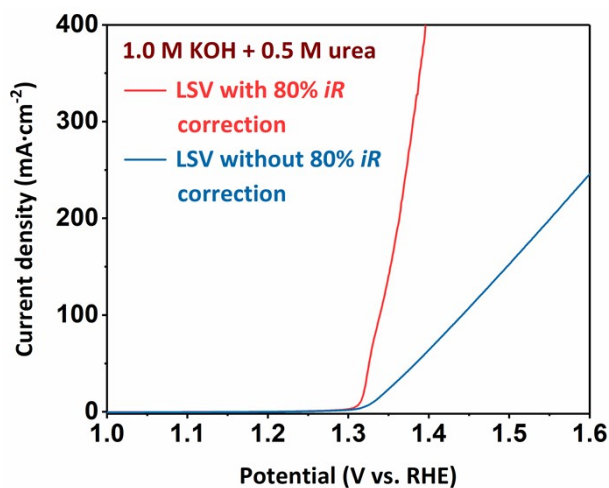**Figure S6.** SEM images of the sample by direct sulfurization from NF.

Figure S7. LSV curves of the Ni_3S_2 catalyst in 1.0 M KOH with 0.5 M urea
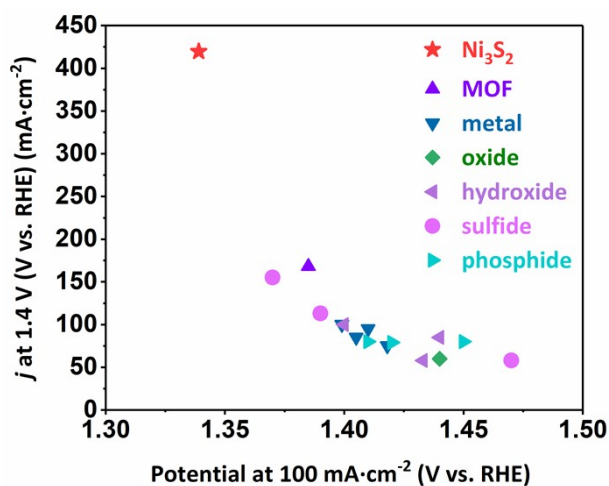
with/without 80% *iR* correction.

Figure S8. Comparison of anodic catalytic activities with different traditional UOR
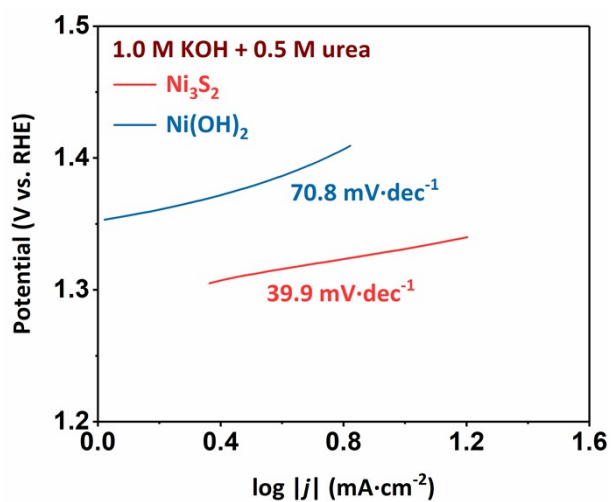
catalysts. The details can be found in **Table S1**.

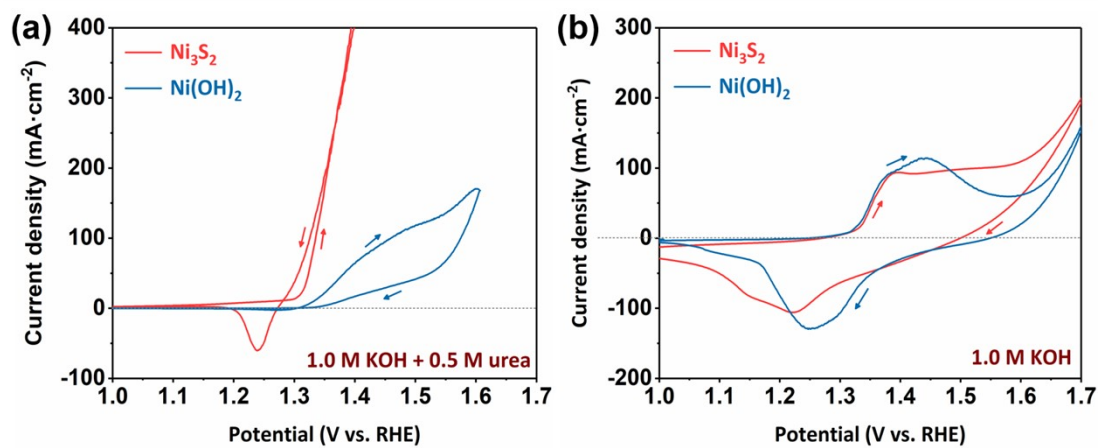**Figure S9.** Tafel plots of Ni(OH)$_2$ and Ni$_3$S$_2$ in 1.0 M KOH with 0.5 M urea.

Figure S10. CV curves of Ni(OH)$_2$ and Ni$_3$S$_2$ in 1.0 M KOH with 0.5 M urea and 1.0 M KOH.
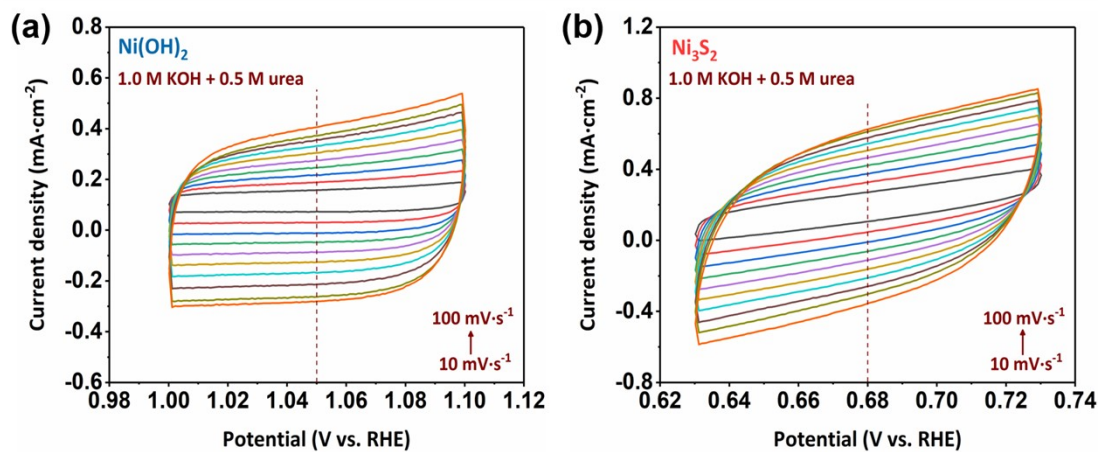
Figure S11. CV curves of Ni(OH)$_2$ and Ni$_3$S$_2$ in the non-faradaic capacitance current region under different scan rates in 1.0 M KOH with 0.5 M urea.
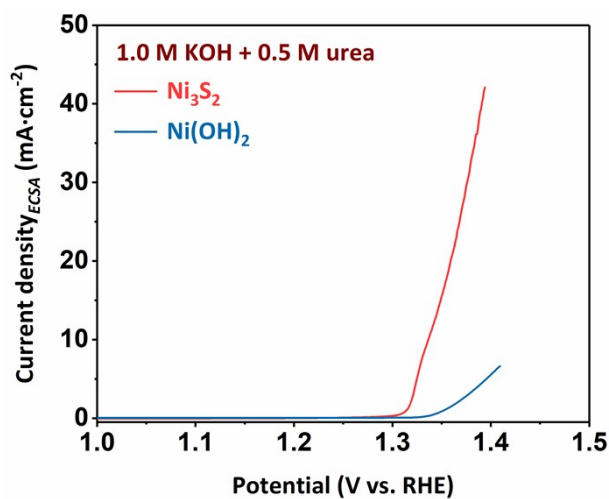

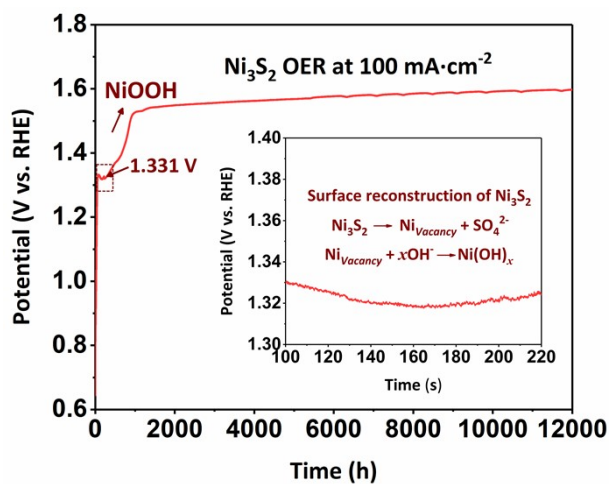**Figure S12.** LSV curves of Ni(OH)$_2$ and Ni$_3$S$_2$ normalized by ECSA.

Figure S13. Chronoamperometry test of the Ni_3S_2 catalyst in 1.0 M KOH under current density of 100 mA·cm^{-2}.
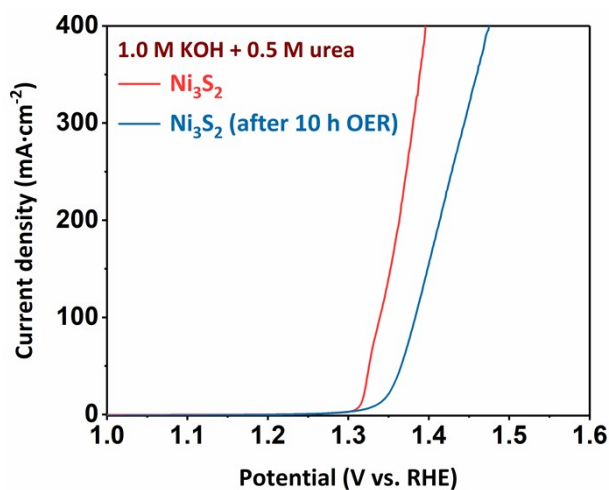

Figure S14. LSV curves of the Ni_3S_2 catalyst before and after OER in 1.0 M KOH with 0.5 M urea.
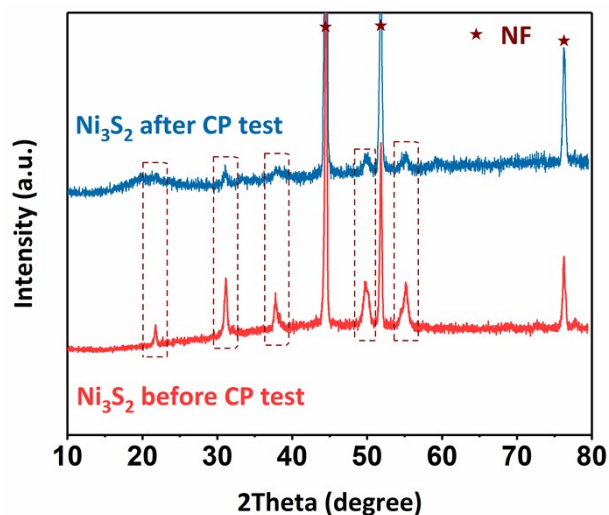
Figure S15. XRD patterns of the Ni_3S_2 catalyst before and after 120 h chronoamperometry test.
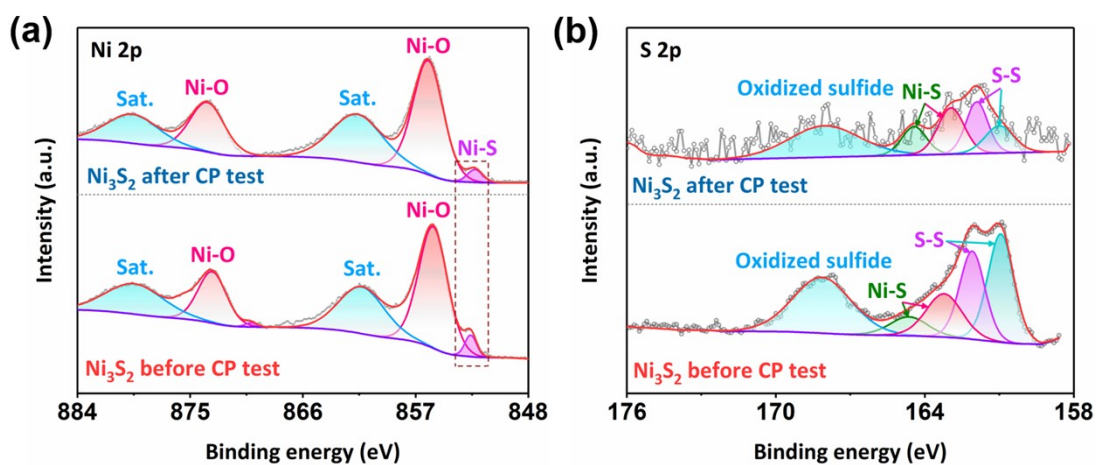

Figure S16. High-resolution (**a**) Ni 2p and (**b**) S 2p spectrum of the Ni_3S_2 catalyst before and after 120 h chronoamperometry test.

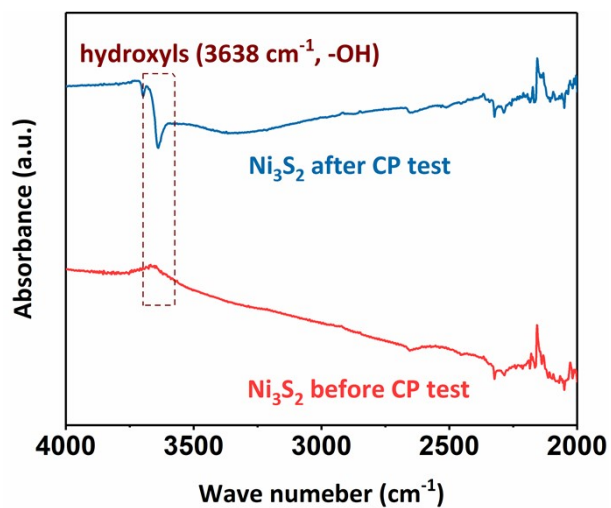**Figure S17.** FTIR spectra of the Ni_3S_2 catalyst before and after 120 h

chronoamperometry test.
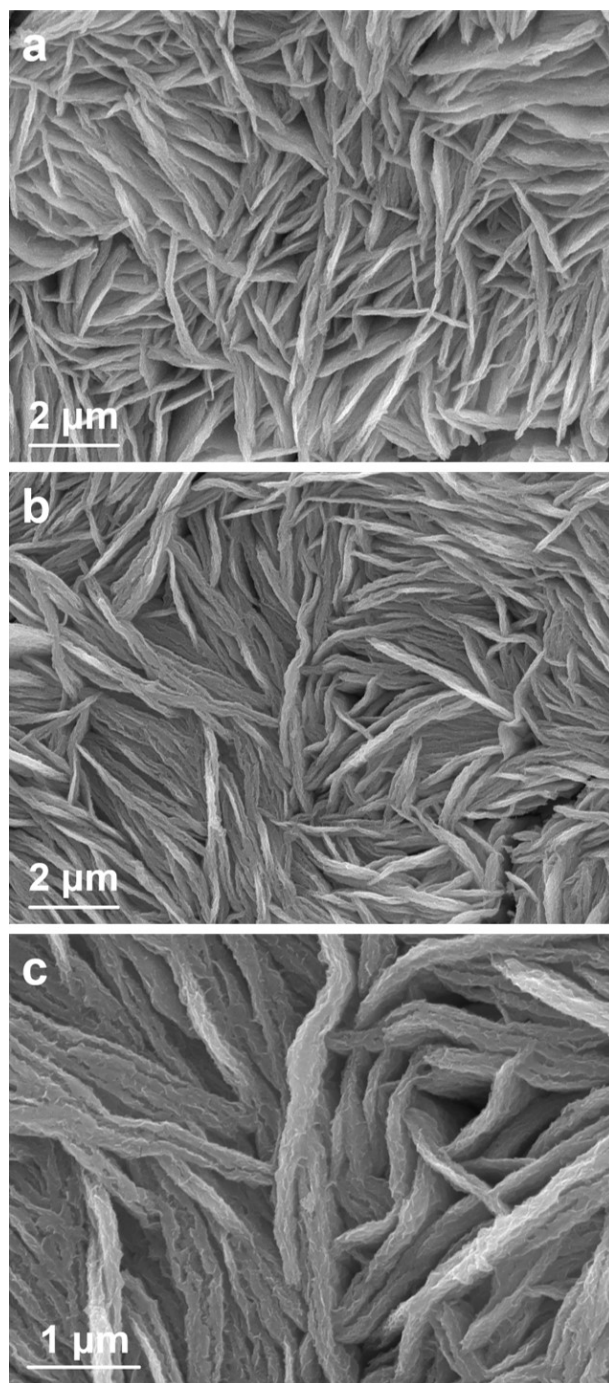
Figure S18. SEM images of the Ni_3S_2 catalyst after 120 h chronoamperometry test.
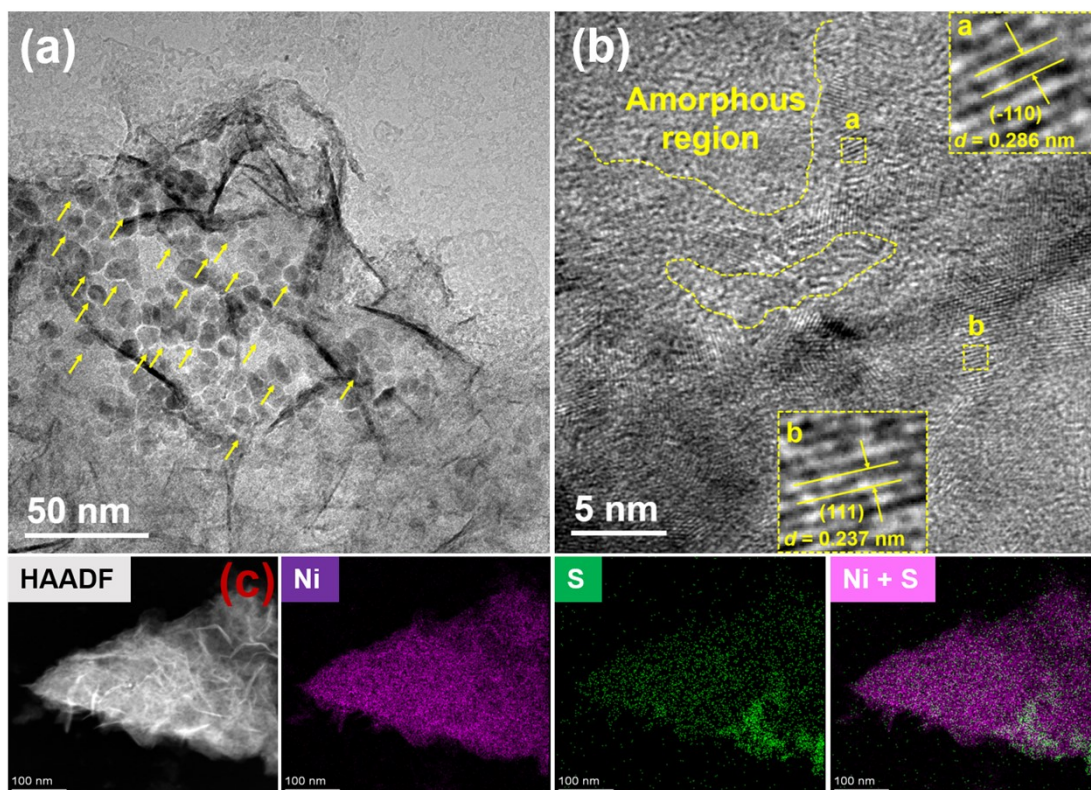
Figure S19. TEM images and corresponding elemental mapping images of the Ni_3S_2 catalyst after 120 h chronoamperometry test.
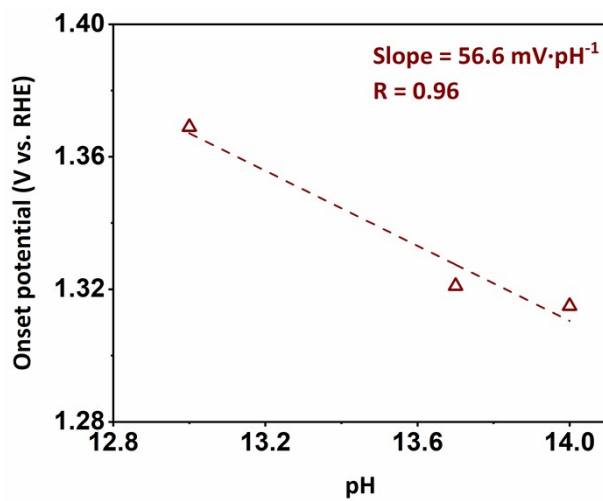
Figure S20. Effect of pH on the onset potential for the Ni_3S_2 catalyst.
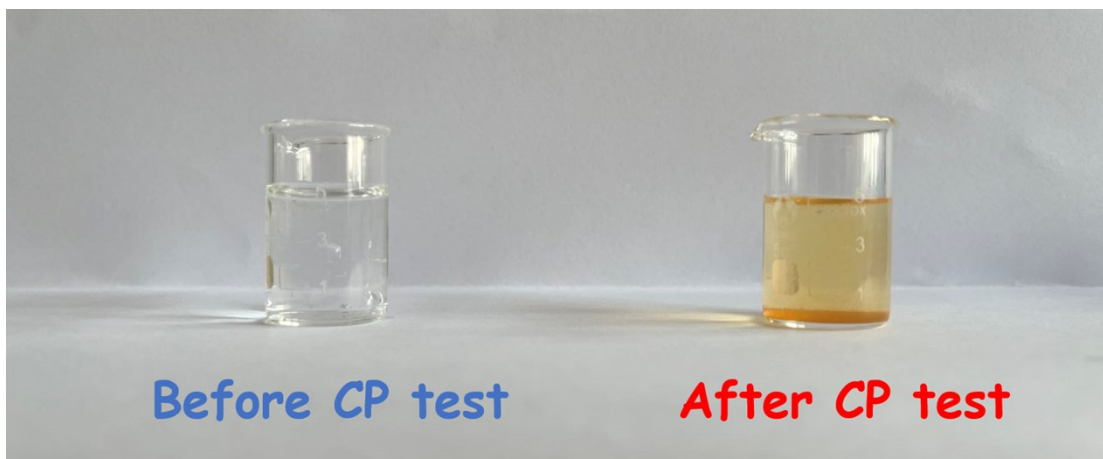
Figure S21. Digital image of the electrolyte after adding the Nessler reagent. Left: the

initial electrolyte. Right: the electrolyte after 40 h chronoamperometry test.
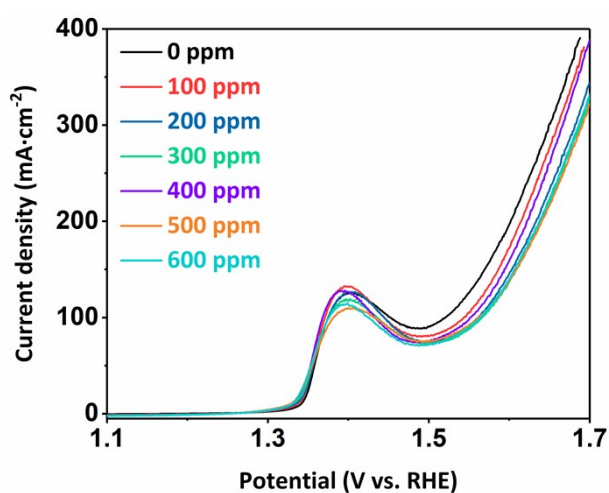
Figure S22. LSV curves of the Ni_3S_2 catalyst in 1.0 M KOH with 100, 200, 300, 400,

500, and 600 ppm of ammonia.
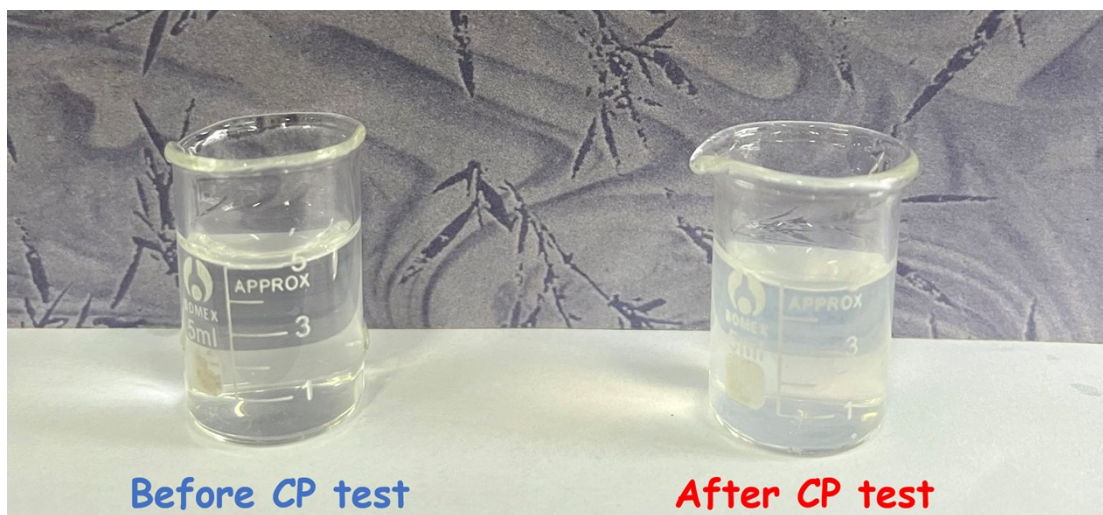
Figure S23. Digital image of the saturated lime water before and after passing into the gas during the anodic reaction. Left: the initial electrolyte. Right: the electrolyte after 40 h chronoamperometry test.
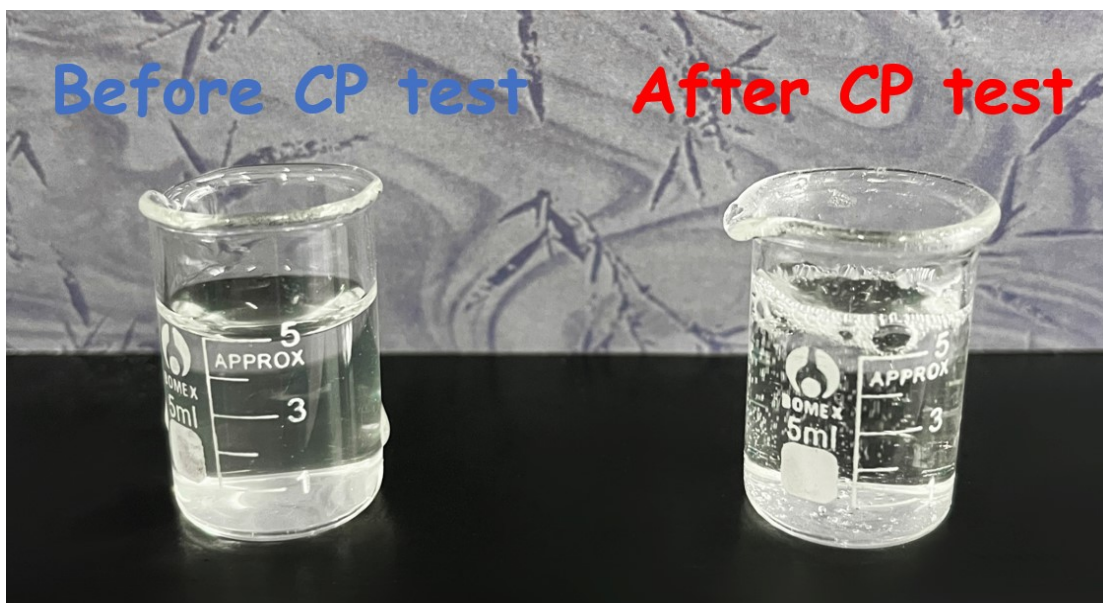
Figure S24. Digital image of the hydrochloric-acidified electrolyte. Left: the initial electrolyte. Right: the electrolyte after 40 h chronoamperometry test.

Figure S25. Digital image of the hydrochloric-acidified electrolyte after adding $BaCl_2$.

Left: the initial electrolyte. Right: the electrolyte after 40 h chronoamperometry test.
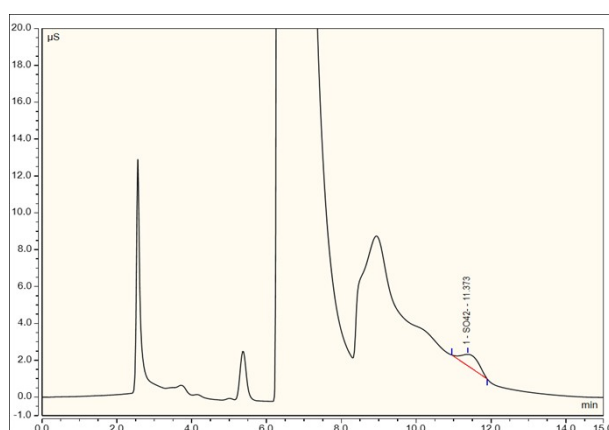
**Figure S26.** Ion chromatography (IC) test to calculate the concentration of SO_4^{2-} ions

in the electrolyte after 40 h chronoamperometry test.
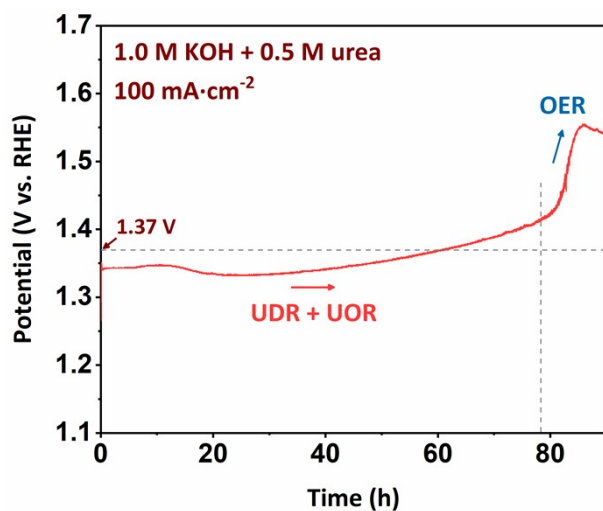
Figure S27. Chronoamperometry test of the Ni_3S_2 catalyst until urea is completely

consumed in 1.0 M KOH with 0.5 M under current density of 100 mA·cm^{-2}.
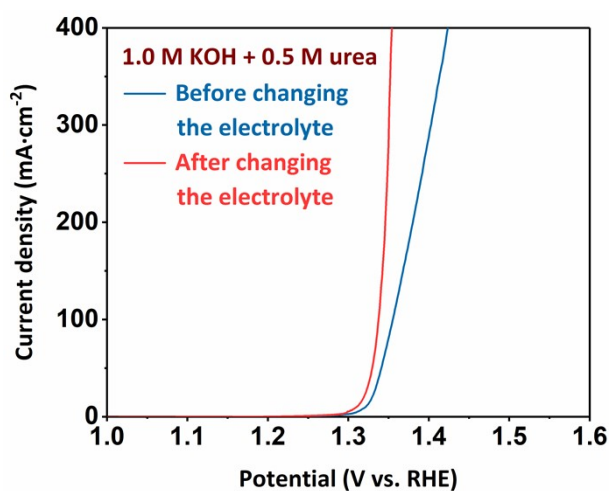
Figure S28. LSV curves of the Ni_3S_2 catalyst before and after changing the

electrolyte.
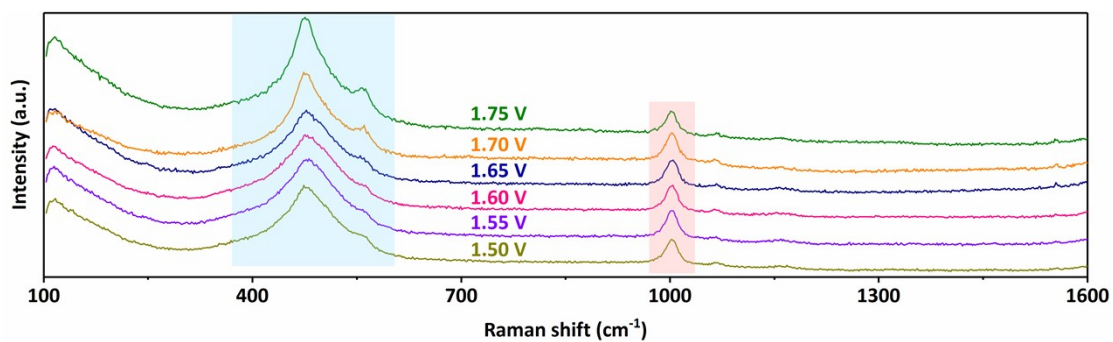
Figure S29. In situ Raman spectra of the Ni_3S_2 catalyst in 1.0 M KOH with 0.5 M urea at high applied potential region.
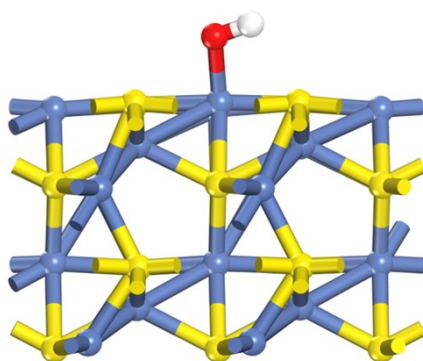
Figure S30. The model of *OH adsorbed on the (002) plane of Ni_3S_2.
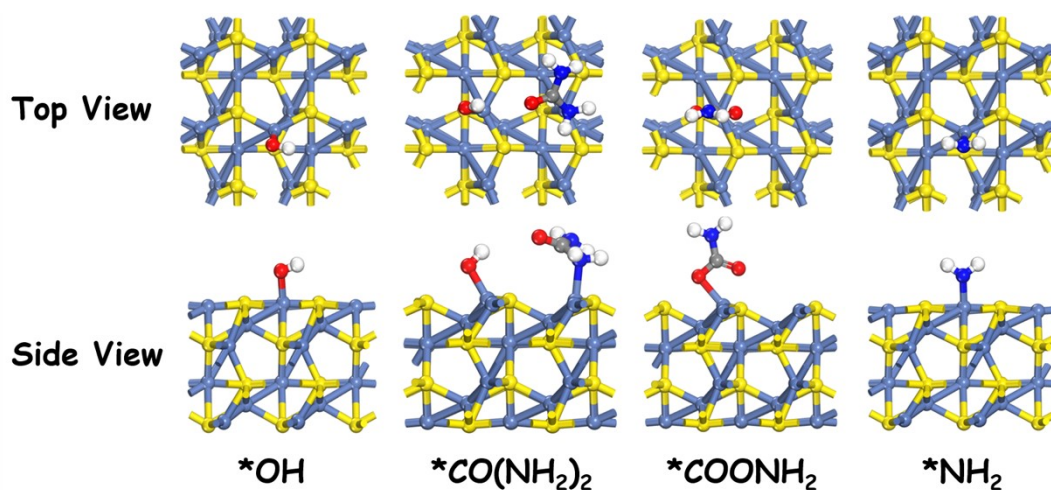
Figure S31. Models of *OH, *CO(NH$_2$)$_2$, *OCONH$_2$ and *NH$_2$ intermidates.
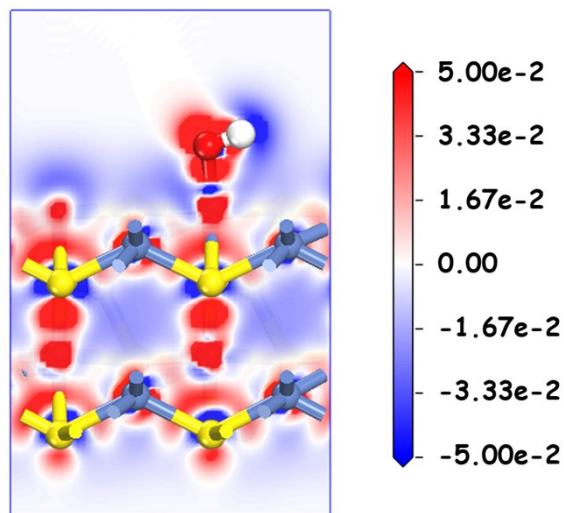
Figure S32. extracted 2D data plot of Ni_3S_2-OH*.
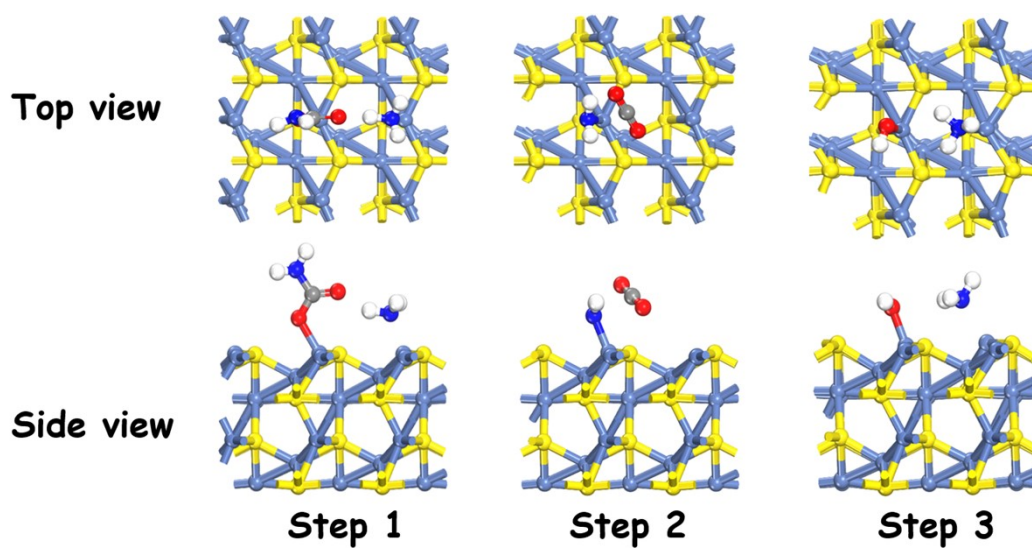
Figure S33. Models of desorption of NH_3 and CO_2 in each step of UDR.
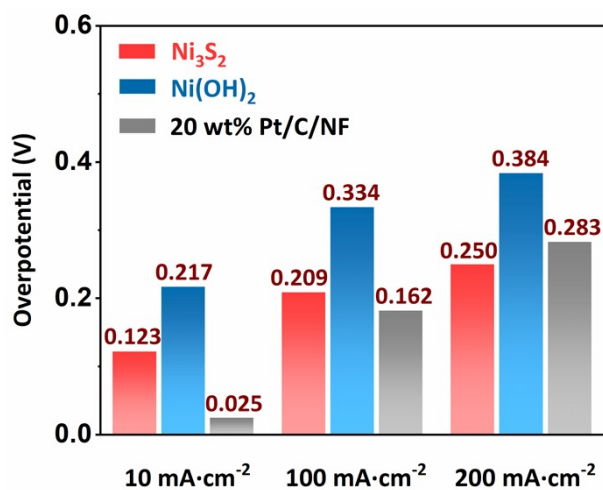
Figure S34. Comparisons of corresponding HER overpotentials required at 10, 100, and 200 mA·cm^{-2} of Ni$_3$S$_2$, Ni(OH)$_2$ and 20 wt% Pt/C/NF in 1.0 M KOH.
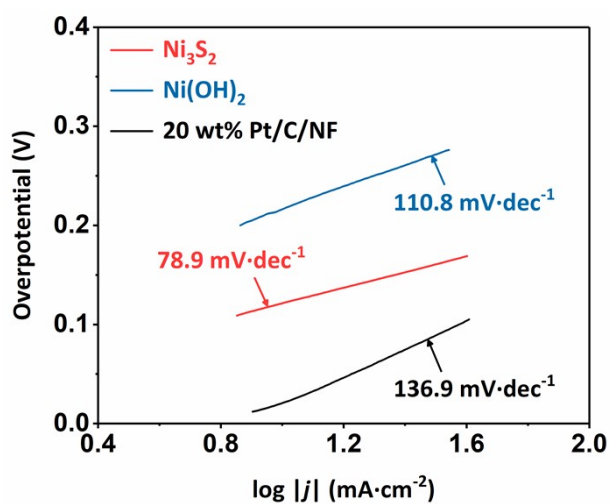
Figure S35. Tafel plots of Ni$_3$S$_2$, Ni(OH)$_2$ and 20 wt% Pt/C/NF in 1.0 M KOH.
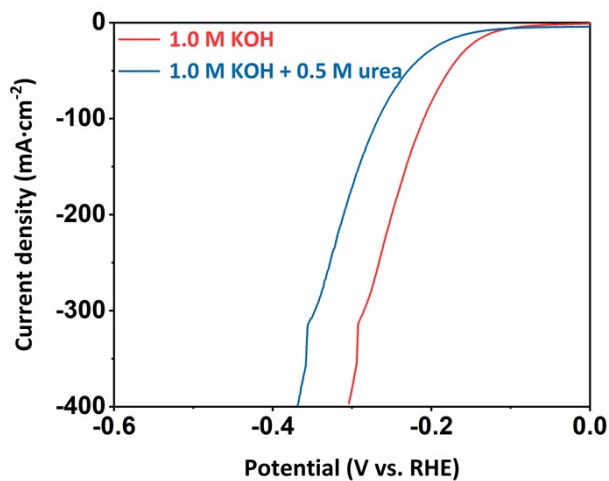
Figure S36. HER LSV curves of the Ni_3S_2 catalyst in 1.0 M KOH and 1.0 M KOH

with 0.5 M urea.
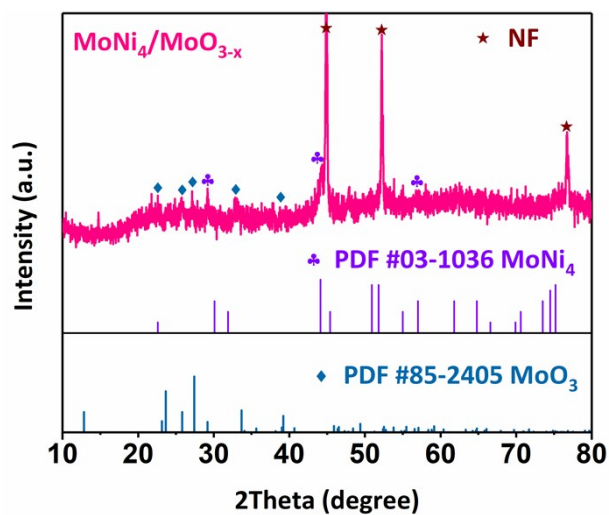
Figure S37. XRD pattern of the $MoNi_4/MoO_{3-x}$ catalyst.
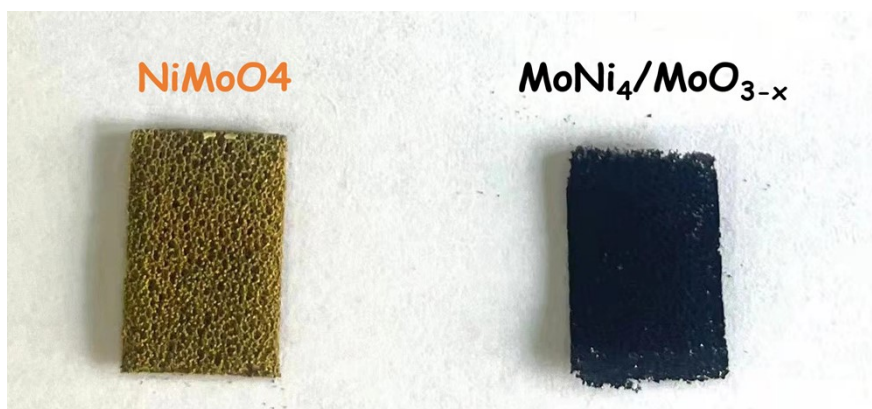
Figure S38. Digital images of $NiMoO_4$ and $MoNi_4/MoO_{3-x}$.
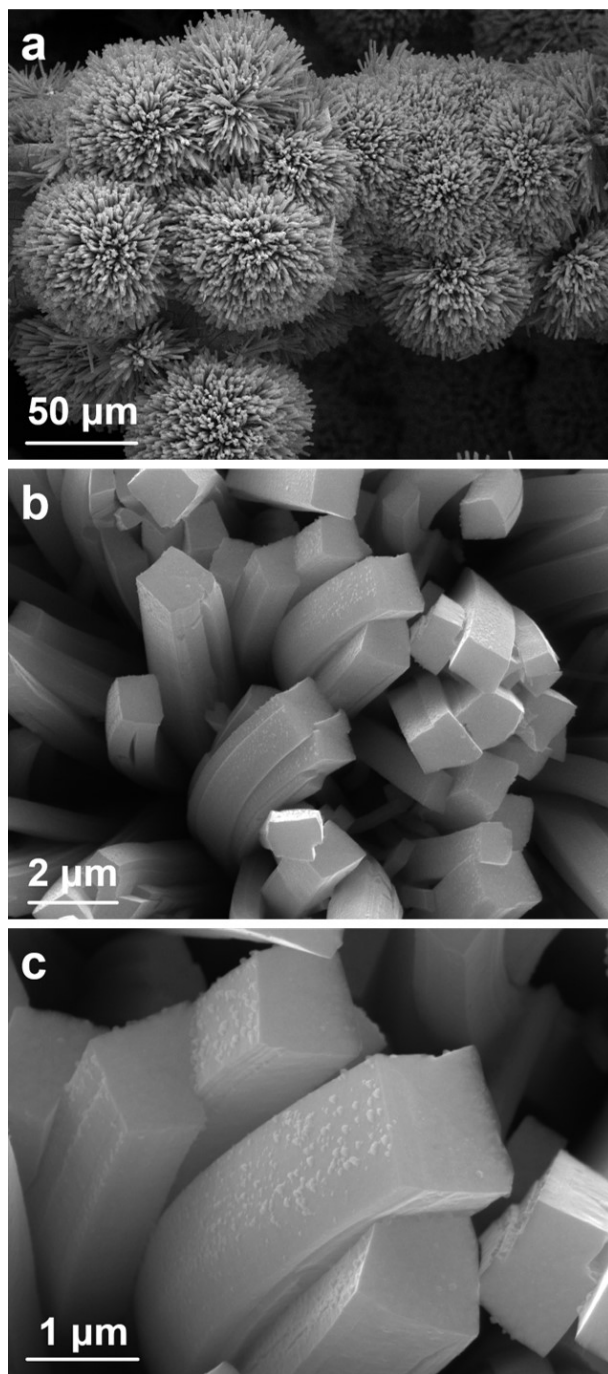
Figure S39. SEM images of the MoNi$_4$/MoO$_{3-x}$ catalyst.
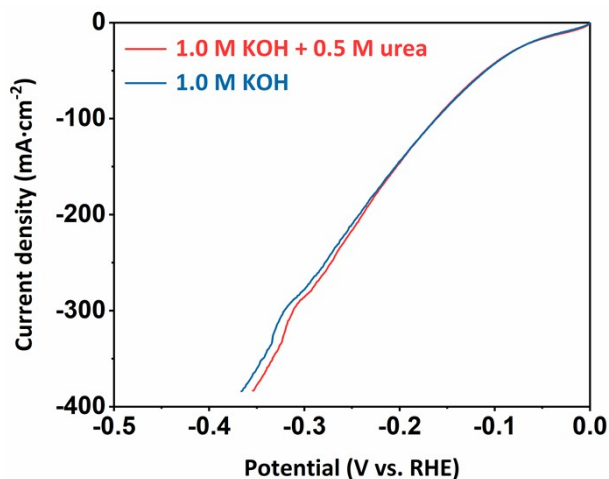
Figure S40. HER LSV curves of the MoNi$_4$/MoO$_{3-x}$ catalyst for HER in 1.0 M KOH

with 0.5 M urea and 1.0 M KOH.
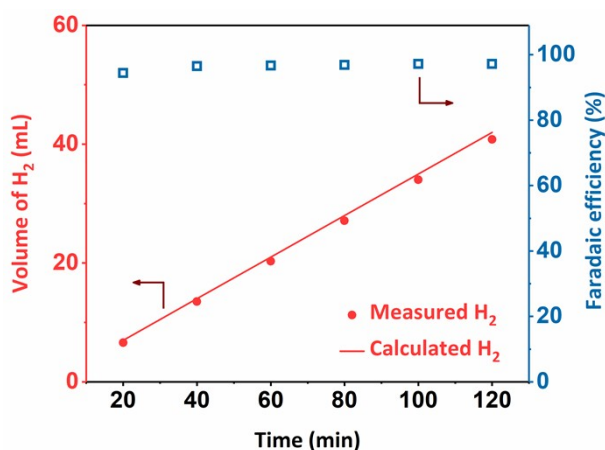
Figure S41. Faradaic efficiency of hydrogen production in the cell system at 50

mA·cm^{-2}.

Table S1. Comparisons of the catalytic activity with recently reported highly efficient

traditional UOR catalysts.

Catalyst	Electrolyte	Potential@100 mA·cm^{-2} (V vs. RHE)	Current density (mA·cm^{-2} @1.4 V)	Catalyst substrate	Ref.

Ni_3S_2	1 M KOH + 0.5 M Urea	1.339	419.6	NF	This work
FeNi-MOF NSs	1 M KOH + 0.33 M Urea	1.385	168	Ti mesh	[3]
Ni_2P@Ni-MOF/NF	1 M NaOH + 0.33 M Urea	1.41	80	NF	[4]
N-$Ni_1Co_3Mn_{0.4}O$/NF	1 M KOH +0.5 M Urea	1.399	100	NF	[5]
NiMoV LDH/NF	1 M KOH + 0.33 M Urea	1.4	100	NF	[6]
NiClO-D	1 M KOH + 0.33 M Urea	1.44	60	Glassy carbon electrode	[7]
$Ni(OH)_2$@NF	1 M KOH + 0.3 M Urea	1.44	85	NF	[8]
N-NiS/NiS_2	1 M KOH + 0.33 M Urea	1.47	58	Carbon cloth	[9]
$NiMoO_4$-$Ni(OH)_2$/NF	1 M KOH + 0.5 M Urea	1.418	75	NF	[10]
r-$NiMoO_4$/NF	1 M KOH +0.5 M Urea	1.41	95	NF	[11]
CuO NWs/CF	1 M KOH + 0.5 M Urea	1.405	85	Cu foam	[12]
CuO Nanobelt	1 M KOH + 0.5 M Urea	1.43	30	Cu foam	[13]
Ni_3S_2-NiS/NF	1 M KOH + 0.5 M Urea	1.37	155	NF	[14]
CA-Ni_5P_4@NiO_x/NF	1 M NaOH + 0.33 M Urea	1.45	80	NF	[15]
Ni_2P/ZnP_4/NF-300	1 M KOH + 0.5 M Urea	1.42	79	NF	[16]
Fe-$NiCo_2S_4$/Ni_3S_2	1 M KOH + 0.5 M Urea	1.39	113	NF	[17]

CoO-Co$_4$N@ NiFe-LDH/NF	1M KOH+ 0.33 M Urea	1.433	58	NF	[18]
CoFe LDH/MOF-0.06/CC	1 M KOH+ 0.33 M Urea	1.57	<20	Carbon cloth	[19]

Table S2. Comparisons of the alkaline urea water splitting performance with recently reported cell systems.

Cell system	Voltage at η_{10} (V)	Ref
Ni$_3$S$_2$ ‖ MoNi$_4$/MoO$_{3-x}$	1.341	This work
H-NiFe-LDH/NF	1.418	[20]
CA-Ni$_5$P$_4$@NiO$_x$/NF	1.53	[15]
Ni$_3$N/Ni$_{0.2}$Mo$_{0.8}$N/NF	1.348	[21]
Ni$_3$S$_2$-Ni$_3$P/NF	1.43	[22]
NCS/NF	1.397	[23]
Cu$_2$S@Ni$_3$Se$_2$	1.48	[24]
Ni-Mn-Se/NF	1.352	[25]
F-Ni(OH)$_2$	1.37	[26]
NiCo$_2$S$_4$/CC	1.45	[27]
NiMoS/NF	1.377	[28]
Fe$_{11\%}$-NiO/NF	1.579	[29]
NiCo MOF/NF-EA	1.477	[30]
FeNi$_3$-MoO$_2$	1.37	[31]
Ni$_2$P/Fe$_2$P/NF	1.47	[32]
NiMoO$_4$	1.38	[33]
P-NiFe@CF	1.37	[34]

NC-FNCP	1.52	[35]
β-NiMoO$_4$	1.633	[36]
Ni(OH)$_2$/NiO-C/WO$_3$ HAs	1.37	[37]
NiS	1.445	[38]
Ni$_3$S$_2$/Ni/NF	1.36	[39]

References

1   J. Perdew, K. Burke, M. Ernzerhof, *Phys. Rev. Lett.*, 1996, **77**, 3865-3868.

2   H. Monkhorst, J. Pack, *Phys. Rev. B*, 1976, **13**, 5188-5192.

3   X. Zhang, X. Fang, K. Zhu, W. Yuan, T. Jiang, H. Xue, J. Tian, *J. Power Sources*, 2022, **520**, 230882.

4   H. Wang, H. Zou, Y. Liu, Z. Liu, W. Sun, K. Lin, T. Li, S. Luo, *Sci. Rep.*, 2021, **11**, 21414.

5   T. Wang, Y. Cao, H. Wu, C. Feng, Y. Ding, H. Mei, *Int. J. Hydro. Energy*, 2022, **47**, 5766-5778.

6   Z. Wang, W. Liu, J. Bao, Y. Song, X. She, Y. Hua, G. Lv, J. Yuan, H. Li, H. Xu, *Chem. Eng. J.*, 2022, **430**, 133100.

7   L. Zhang, L. Wang, H. Lin, Y. Liu, J. Ye, Y. Wen, A. Chen, L. Wang, F. Ni, Z. Zhou, S. Sun, Y. Li, B. Zhang, H. Peng, *Angew. Chem. Int. Ed.*, 2019, **58**, 16820-16825.

8   L. Xia, Y. Liao, Y. Qing, H. Xu, Z. Gao, W. Li, Y. Wu, *ACS Appl. Energy Mater.*, 2020, **3**, 2996-3004.

9   H. Liu, Z. Liu, F. Wang, L. Feng, *Chem. Eng. J.*, 2020, **397**, 125507.

10   S. Hu, H. Wu, C. Feng, Y. Ding, *Int. J. Hydro. Energy*, 2020, **45**, 21040-21050.

11   Y. Tong, P. Chen, M. Zhang, T. Zhou, L. Zhang, W. Chu, C. Wu, Y. Xie, *ACS Catal.*, 2018, **8**, 1-7.

12   H. Sun, J. Liu, G. Chen, H. Kim, S. Kim, Z. Hu, J. Chen, S. Haw, F. Ciucci, W. Jung, *Small Methods*, 2022, **6**, 2101017.

13   Y. Wang, Y. Li, L. Ding, J. Ding, *Chem. Commun.*, 2019, **55**, 13562-13565.

14   Q. Zhao, C. Meng, D. Kong, Y. Wang, H. Hu, X. Chen, Y. Han, X. Chen, Y. Zhou, M. Lin, M. Wu, *ACS Sustain. Chem. Eng.*, 2021, **9**, 15582-15590.

15   Z. Ma, H. Wang, H. Ma, S. Zhan, Q. Zhou, *Fuel*, 2022, 315, 123279.

16   R. Wang, T. Wnag, C. Feng, H. Wu, Y. Ding, H. Me, *Int. J. Hydro. Energy*, 2021, 46, 38247-38257.

17   Y. Wang, N. Chen, X. Du, X. Han, X. Zhang, *J. Alloys Compd.*, 2022, 893, 162269.

18   B. Chen, M. Humayun, Y. Li, H. Zhang, H. Sun, Y. Wu, C. Wang, *ACS Sustain. Chem. Eng.*, 2021, **9**, 14180-14192.

19   S. Huang, Y. Wu, J. Fu, P. Xin, Q. Zhang, Z. Jin, J. Zhang, Z. Hu, Z. Chen, *Nanotechnology*, 2021, **32**, 385405.

20   L. Chen, H. Wang, L. Tan, D. Qiao, X. Liu, Y. Wen, W. Hou, T. Zhan, *J. Colloid Inter. Sci.*, 2022, **618**, 141-148.

21   R. Li, X. Wan, B. Chen, R. Cao, Q. Ji, J. Deng, K. Qu, X. Wang, Y. Zhu, *Chem. Eng. J.*, 2021, **409**, 128240.

22   J. Liu, Y. Wang, Y. Liao, C. Wu, Y. Yan, H. Xie, Y. Chen, *ACS Appl. Mater. Inter.*, 2021, **13**, 26948-26959.

23   W. Liu, L. Dai, Y. Hu, K. Jiang, Q. Li, Y. Deng, J. Yuan, J. Bao, Y. Lei, *Inorg. Chem. Front.*, 2021, **8**, 4528-4535.

24   L. Lv, Z. Li, H. Wan, C. Wang, *J. Colloid Inter. Sci.*, 2021, **592**, 13-21.

25   M. Maleki, G. Darband, A. Rouhaghdam, R. Andaveh, Z. Kazemi, *Chem. Commun.*, 2022, **58**, 3545-3548.

26   S. Patil, N. Chodankar, S. Hwang, G. Raju, Y. Huh, Y. Han, *Small*, 2022, **18**, 2103326.

27   W. Song, M. Xu, X. Teng, Y. Niu, S. Gong, X. Liu, X. He, Z. Chen, *Nanoscale*, 2021, **13**, 1680-1688.

28   F. Wang, K. Zhang, Q. Zha, Y. Ni, *J. Alloys Compd.*, 2022, **899**, 163346.

29   Z. Wu, Z. Zou, J. Huang, F. Gao, *J. Catal.*, 2018, **358**, 243-252.

30   D. Wei, W. Tang, N. Ma, Y. Wang, *J. Alloys Compd.*, 2021, **874**, 159945.

31   Q. Xu, T. Yu, J. Chen, G. Qian, H. Song, L. Luo, Y. Chen, T. Liu, Y. Wang, S. Yin, *ACS*

Appl. Mater. Inter. 2021, **13**, 16355-16363.

32   L. Yan, Y. Sun, E. Hu, J. Ning, Y. Zhong, Z. Zhang, Y. Hu, *J. Colloid Inter. Sci.*, 2019, **541**, 279-286.

33   Z. Yu, C. Lang, M. Gao, Y. Chen, Q. Fu, Y. Duan, S. Yu, *Energy Environ. Sci.*, 2018, **11**, 1890-1897.

34   W. Yun, G. Das, B. Kim, B. Park, H. Yoon, Y. Yoon, *Sci. Rep.*, 2021, **11**, 22003.

35   J. Zhang, S. Huang, P. Ning, P. Xin, Z. Chen, Q. Wang, K. Uvdal, Z. Hu, *Nano Res.*, 2022, **15**, 1916-1925.

36   K. Hu, S. Jeong, G. Elumalai, S. Kukunuri, J. Fujita, Y. Ito, *ACS Appl. Energy Mater.*, 2020, **3**, 7535-7542.

37   J. Zhao, Y. Zhang, H. Guo, J. Ren, H. Zhang, Y. Wu, R. Song, *Chem. Eng. J.*, 2022, **433**, 134497.

38   M. Zhong, W. Li, C. Wang, X. Lu, *Appl. Surf. Sci.*, 2022, **575**, 151708.

39   X. Zhuo, W. Jiang, G. Qian, J. Chen, T. Yu, L. Luo, L. Lu, Y. Chen, S. Yin, *ACS Appl. Mater. Inter.* 2021, **13**, 35709-35718.